Actin Dynamics at the Living Cell Submembrane Imaged by Total Internal Reflection Fluorescence Photobleaching

Susan E. Sund and Daniel Axelrod
Department of Physics and Biophysics Research Division, University of Michigan, Ann Arbor, Michigan 48109 USA

ABSTRACT Although reversible chemistry is crucial to dynamical processes in living cells, relatively little is known about relevant chemical kinetic rates in vivo. Total internal reflection/fluorescence recovery after photobleaching (TIR/FRAP), an established technique previously demonstrated to measure reversible biomolecular kinetic rates at surfaces in vitro, is extended here to measure reversible biomolecular kinetic rates of actin at the cytofacial (subplasma membrane) surface of living cells. For the first time, spatial imaging (with a charge-coupled device camera) is used in conjunction with TIR/FRAP. TIR/FRAP imaging produces both spatial maps of kinetic parameters (off-rates and mobile fractions) and estimates of kinetic correlation distances, cell-wide kinetic gradients, and dependences of kinetic parameters on initial fluorescence intensity. For microinjected rhodamine actin in living cultured smooth muscle (BC3H1) cells, the unbinding rate at or near the cytofacial surface of the plasma membrane (averaged over the entire cell) is measured at $0.032 \pm 0.007\ s^{-1}$. The corresponding rate for actin marked by microinjected rhodamine phalloidin is very similar, $0.033 \pm 0.013\ s^{-1}$, suggesting that TIR/FRAP is reporting the dynamics of entire filaments or protofilaments. For submembrane fluorescence-marked actin, the intensity, off-rate, and mobile fraction show a positive correlation over a characteristic distance of 1–3 μm and a negative correlation over larger distances greater than ~7–14 μm. Furthermore, the kinetic parameters display a statistically significant cell-wide gradient, with the cell having a "fast" and "slow" end with respect to actin kinetics.

INTRODUCTION

Active cellular processes involving morphology, such as endo- and exocytosis, ruffling, lamellipodial extension, and cell motility, probably require reversibility in the binding events among submembrane structural proteins and lipids. However, few techniques are available for measuring or imaging in vivo binding/unbinding kinetic rates of proteins in cells. Standard nonimaging techniques for measuring kinetics rates in vitro, such as stop flow, concentration jumps, pressure jumps, and temperature jumps, are difficult to apply to single living cells. Total internal reflection/fluorescence recovery after photobleaching (TIR/FRAP), as described below, is shown in this study to measure and spatially map the varied submembrane binding kinetic rates of fluorescence-marked actin in living cells.

TIR fluorescence (TIRF) is an optical technique used to excite fluorophores within ~80 nm of a water-glass or cell-glass interface (Axelrod et al., 1992). The illumination intensity decays exponentially with distance from the surface with a characteristic length that depends on the illumination angle, indices of refraction at the interface, and illuminating wavelength. When applied to a living cell adhering to a coverslip and injected with a fluorescent actin marker, TIRF preferentially excites fluorophores at or near the plasma membrane at the cell-glass contact regions, while not exciting fluorophores deeper in the cytosol (see Fig. 1).

TIRF combined with FRAP can measure kinetic rates of fluorescent molecules in reversible equilibrium with binding sites at a surface (Thompson et al., 1981). TIR/FRAP previously has been used to measure unbinding rates (also called "off-rates") of cytoplasmic proteins (McKiernan et al., 1997) and immune system proteins (Hsieh and Thompson, 1995; Sheets et al., 1997; Gesty-Palmer and Thompson, 1997) from supported lipid bilayers, and the unbinding rates of hormones from biological cell surfaces (Hellen and Axelrod, 1991; Fulbright and Axelrod, 1993), all in nonliving systems and in a nonimaging mode.

In this paper, actin in living BC3H1 (mouse smooth muscle-like) cells is fluorescently labeled by microinjection of either rhodamine-labeled g-actin or rhodamine-labeled phalloidin (a toxin that binds strongly to f-actin). Actin kinetics are measured by TIR/FRAP in the presence or absence of cytochalasin B (which blocks monomer association/disassociation at the barbed (fast) end of actin polymers; MacLean-Fletcher and Pollard, 1980; Cooper, 1987), sodium azide and 2-deoxyglucose (which block ATP production), and unlabeled phalloidin. Rhodamine-phalloidin kinetics are also measured in the absence of further treatment. The spatially resolved kinetic data are displayed as spatial maps ("images") and analyzed by spatial autocorrelations, linear gradient fits, and dependence on initial intensity. We find that the average off-rate of actin is spatially nonuniform and sensitive to drug treatments. The optical and analysis techniques used here should be generally applicable to many other membrane or submembrane binding proteins.

Actin kinetics near the membrane may result from several phenomena: binding/unbinding of a polymerized f-actin fil-

Received for publication 3 January 2000 and in final form 14 June 2000.
Address reprint requests to Dr. Daniel Axelrod, Biophysics Research Division, University of Michigan, 930 North University St., Ann Arbor, MI 48109-1055. Tel.: 734-764-5280; Fax: 734-764-3323; E-mail: daxelrod@umich.edu.

Dr. Sund's present address is Raytheon ITSS, Pasadena, CA 91101.

0006-3495/00/09/1655/15 $2.00

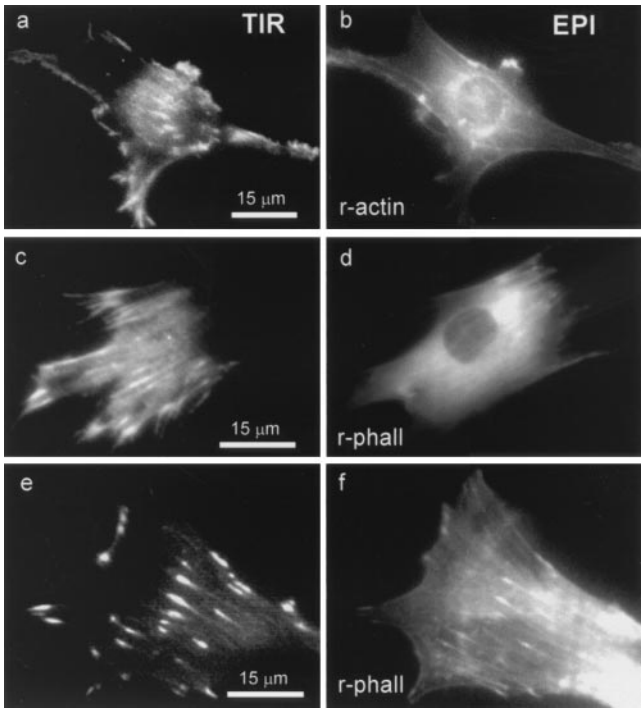

FIGURE 1 TIR versus EPI illumination on living BC3H1 cells injected with R-actin (*a* and *b*) or R-phalloidin (*c– f*). TIR illumination (*a, c,* and *e*) excites the fluorescence-marked actin selectively near the plasma membrane at cell-substrate contact regions. EPI illumination (*b, d,* and *f*) shown for the same cells excites the fluorescence-marked actin throughout the entire cell. Comparison of TIR versus EPI shows, for example, that the right side of the cell in *c* is not attached to the coverslip; a phase-contrast image (not shown) shows an adjacent nonfluorescent cell on the right, presumably intercolated into the substrate-proximal space under the fluorescent cell.

ament side or tip to any of dozens of membrane-anchoring proteins or protein complexes in the membrane, binding of monomeric g-actin to specific anchoring proteins, binding of either type of actin directly to membrane lipids, or exchange of monomers at the filament tip. F-actin binding directly to lipid has been detected in vitro, using differential scanning calorimetry and electron microscopy, and in ionic conditions found in vivo (Gicquaud, 1993, 1995). Rates of turnover in actin filaments in the cytosol of Swiss 3T3 cells, fibroblast cell lines, and goldfish epithelial keratocytes have previously been measured by Wang (1987), Theriot and Mitchison (1992), and Tardy et al. (1995), using FRAP and fluorescent photoactivation techniques in non-TIR modes.

MATERIALS AND METHODS

Biological preparation

The cell chamber consisted of a 35-mm plastic culture dish with a ¾″ diameter hole drilled out and a cleaned coverslip glued over it onto the outside of the dish with Sylgard 182 epoxy resin (Dow Corning Corp., Midland, MI). Coverslips were previously cleaned by boiling in a porcelain holder in 5% Linbro 7× cleaning solution (Flow Laboratories, McLean, VA) for at least 45 min, followed by rinsing in running deionized water, dipping in acetone three times, and heating at 110–150°C to dryness for several hours.

BC3H1 cells are flat, adherent, irregularly shaped cells on the order of 50 μm across that are a few microns thick at most in extranuclear regions. Injected BC3H1 cells were plated directly into the glass-bottomed dishes described above by standard procedures and incubated for at least 2 days at 37°C, 9% CO_2 in Dulbecco's modified Eagle's medium containing 10% heat-inactivated fetal bovine serum (GIBCO, Grand Island, NY). Before microinjection, the medium was replaced with room temperature Dulbecco's phosphate-buffered saline with 1 g/liter glucose (PBSg) (GIBCO).

Microinjection protocol

Cell microinjection was performed on a Leitz Diavert moving stage focus microscope; the same microscope was used for the subsequent optical observations. The entire microinjection positioner setup (as custom-assembled from standard precision translators) was firmly bolted to a microscope support column that moves vertically along with the stage focus mechanism. Starting from the bolting point, the setup consisted of a mechanical *x-y-z* translator (Line Tool Co., Allentown, PA) onto which was mounted a piezoelectric transducer (Physik Instruments, Costa Mesa, CA) driven by a standard 24-V power supply. To prevent sheer forces on the piezotranslator, the moving end of the piezoelectric transducer was glued to the moving platform of a one-dimensional miniature ball slider (model 0611; Daedel, Harrison City, PA), the frame of which was fixed to the *x-y-z* translator. A universal joint that held a micropipette holder/pressure tubing assembly (General Valve, Fairfield, NJ) was affixed to the ball slider's moving platform.

Microinjection pipettes (with filaments) were pulled with a Flaming Brown pipette puller (Sutter Instrument, Novato, CA) to a tip inside diameter of ~0.2 μm. Continuous rather than pulse pressure, at 5–20 psi, was used during injection to prevent pipette clogging. Also to prevent pipette clogging, the protein was prefiltered through a 0.22-μm centrifuge filter tube (SpinX; Costar, Cambridge, MA) at ~1000 × *g* for 5 min. The injection solution was delivered into about four pipettes (with the delivery close to the pipette tip to prevent clogging) with a 5-μl Hamilton syringe (Hamilton Company, Reno, NV). After each use, the syringe was cleaned with ethanol and blown out with nitrogen gas. After the pipette was swung into place on the universal joint and the tip was centered in the field of view, using a 3× objective and darkfield illumination, the pipette tip was brought down with the mechanical translator to touch the cell membrane. With a 40× phase-contrast objective, a dimple could be seen where the pipette touched the membrane. The piezoelectric translator was then transiently powered to give the pipette a ~2-μm fast poke. A ripple throughout the cell indicated that liquid was injected. A slow, contained ripple was found to correlate with probable cell survival, whereas a faster, more violent ripple was found to correlate with probable cell death. If the injection was judged as good, the cell coordinates were recorded. Fig. 2 shows phase-contrast images of several BC3H1 cells, two of which were microinjected. Actin is particularly difficult to microinject because it tends to polymerize where the injection solution contacts the cell buffer solution; after the pipette clogged, it was sometimes intentionally broken on the coverslip and further used at a lower pressure.

Injection solutions

Three different protein combinations were microinjected, which were prepared as follows.

Rhodamine actin

Actin was purified from rabbit skeletal muscle by the method of Pardee and Spudich (1982). Actin was labeled by reaction with tetramethylrhodamine

iodoacetamide by the procedure of Simon et al. (1988). The final actin concentration was 30–100 μM, with ~50% labeled actin, and was stored at −70°C. The labeled actin was used within 1 h of being thawed and filtered.

Rhodamine phalloidin

Rhodamine phalloidin was obtained from Molecular Probes (Eugene, OR) and stored in a stock concentration of methanol recommended by Molecular Probes, at ~6 μM at −20°C. For microinjection, the stock solution was ~90% evaporated under nitrogen and reconstituted at 6–12 μM in deionized water. In this form, stored at 10°C, it could be used for up to several days without refiltering.

Rhodamine actin and unlabeled phalloidin

Unlabeled phalloidin from Molecular Probes was stored in a stock solution of ~46 μM in methanol at −20°C and was added without evaporation to rhodamine actin before filtering in a 1:8 (v/v) ratio for microinjection.

Biochemical disruption treatments

Some of the rhodamine-actin-labeled cell dishes were subject to specific biochemical disruption. Disruptive treatments consisted of 50 μl of one of the following stock solutions added to the 2 ml of PBSg already on the cells and triturated ~20 times: 1) cytochalasin B stock solution (5 mg of cytochalasin B in 1.25 ml ethanol, stored at −20°C; 0.1 mg/ml final concentration of cytochalasin B, a concentration more than sufficient to totally disrupt actin filaments) or 2) sodium azide stock solution (5 ml of H_2O, 0.33 g of 2-deoxyglucose, 0.13 g of sodium azide, and 0.06 g of NaCl; 10 mM final concentration of both sodium azide and 2-deoxyglucose). For nondisrupted controls, the same solvents (ethanol or 100 mM NaCl) were added to cells in the same volume but without the cytochalasin or sodium azide solutes. No significant differences were seen between the ethanol-based and NaCl-based controls, so results for these two preparations are pooled where averaging is appropriate.

Postinjection protocol

After microinjection of many cells in one dish under dim epiillumination, the cell PBSg was replaced by 2 ml of fresh PBSg. A layer of mineral oil on top of the PBSg prevented evaporation. In this preparation, cells have been observed to live for more than 1 day. At least 15 min after injection, one injected cell was selected based on viable appearance in phase contrast and an acceptable amount of fluorescence gauged with dim epiillumination. In the case of rhodamine-actin-injected cells, a coin was flipped to randomly determine whether the cell dish would receive a disruptive treatment or control treatment as above. TIR/FRAP experiments were carried out at least 1 h after treatment with a computer-controlled laser/charge-coupled device (CCD) setup. All experiments were performed at 25°C. During or after the TIR/FRAP experiment, a phase-contrast time lapse movie (at 2 frames/min) of at least 15 min duration was taken to assay cell viability. A cell was defined to be "alive" if one or more lamellipodia were extended during the 15-min observation period.

The results are based on experiments on seven "control" rhodamine-actin-injected cells left untreated by disruptive agents, three rhodamine-actin-injected cells treated with cytochalasin B, three rhodamine-actin-injected cells treated with azide solution, five rhodamine-actin-injected cells treated with unlabeled phalloidin, and five rhodamine-phalloidin-injected cells. Of these, most were also used for spatial analysis, although some cells were too noisy or ill behaved for spatial analysis.

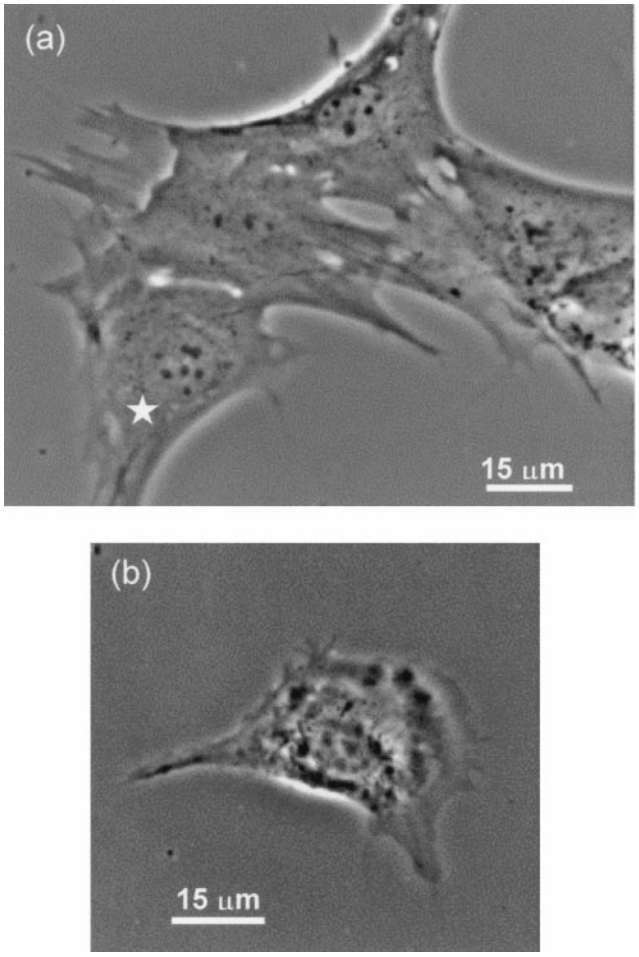

FIGURE 2 Phase-contrast images of BC3H1 cells. (*a*) A field showing a rhodamine-actin-injected cell (marked by a *star*), with several other uninjected cells nearby. The injected cell was among those used for data acquisition (cell *a* of Fig. 5). (*b*) Another rhodamine-actin-injected cell used for data acquisition (cell *e* of Fig. 5).

Cell fixation

For rhodamine-actin-labeled fixed cells, cells were microinjected and incubated for 1 h, then fixed according to the method of Bloch et al. (1989). Rhodamine-phalloidin-labeled fixed cells were fixed according to the method of Bloch et al., then labeled with 5 μl of rhodamine phalloidin methanol stock solution in 200 μl PBSg.

Optical setup

A 3-W CW argon laser (model 2020; Spectra Physics, Mountain View, CA) was used to provide excitation at 514.5 nm. An acoustooptical modulator and a solenoid-operated shutter controlled the laser illumination duration. The laser was focused by a 9-cm focal length lens to an elliptical region 40 μm wide and 100 μm long. All experiments were conducted with a power of ~0.04 W incident upon the cell substrate surface. Our novel TIR setup, shown in Fig. 3, was specially designed to 1) allow complete access to the cells by a microinjection pipette from above and 2) provide the large incidence angle needed for TIR in cell-glass interfaces. This setup requires the use of an air or water immersion objective. ("Prismless" (through-the lens) TIR excitation with a 1.4 NA objective (Stout and

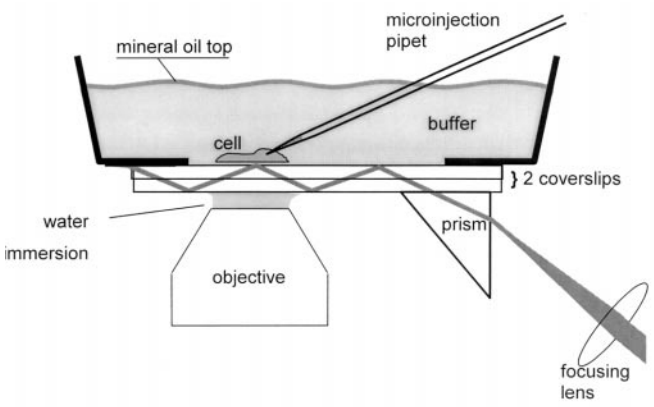

FIGURE 3 TIR optical setup and cell chamber. Our TIR optical setup uses two no. 2 coverslips and an inexpensive commercial 45–45-90° triangular prism (7-mm sides, refractive index = 1.52). The top coverslip, to which the cells are adhered, is glued to the bottom of a drilled-out 35-mm plastic tissue culture dish with Sylgard 182 encapsulating resin (Exxex Group, Wood Dale, IL). The bottom coverslip is in optical contact with both the top coverslip above and the prism below through thin layers of immersion oil. For searching the cell culture in the horizontal plane with the standard microscope stage translators, the dish-coverslip configuration slides freely with respect to the prism, which is prepositioned below the stage by a three-dimensional translator attached to the microscope but otherwise held fixed. (Another possibility is to keep the lower coverslip fixed relative to the prism and allow only the upper coverslip to slide horizontally; this would minimize oil smearing when the sample is moved.) The laser beam enters the coverslips through the prism at a ~75° incidence angle. Once trapped inside the coverslips, the beam totally internally reflects several times. The relatively thick double coverslip combination allows successive reflections to be well separated, but it is not so thick as to preclude the use of moderately short working distance objectives. The third or fourth reflection at the upper surface was used in these experiments. This setup requires an intermediate or long working distance water-immersion or air objective (an oil immersion lens would prevent TIR at the immersion-coverslip interface). (A Leitz achromat (50×, NA 1.00, free working distance 0.68 mm, 160-mm tube length) was used here.) In contrast to other inverted microscope prism-based TIR configurations, this TIR setup has the advantages of 1) providing complete access to the cell from above and 2) presenting the sample at the immediate far side of a coverslip (rather than through an additional layer of medium beyond the coverslip), which reduces optical aberrations.

Axelrod, 1989) also allows an open access chamber, but it does not provide an incidence angle significantly greater than the TIR critical angle for viewing the cytoplasm. However, recently commercialized objectives of 1.45 and 1.65 NA avoid this problem (Axelrod, 2000).) To maximize emission light throughput, the microscope dichroic mirror (which is standard for epifluorescence) was removed because it is not necessary for TIR.

Data acquisition

Data were collected with a CCD camera (Photometrics Star 1, Tucson, AZ). Data acquisition was automated and was controlled with a custom-written PC program and hardware consisting of a CTR-05 counter-timer board (Computer Boards, Inc.) interfaced to the acoustooptical modulator and laser shutter, and a GPIB board (National Instruments, Austin, TX) interfaced to the camera. The probe excitation light was provided as a flash of 1/60 s duration (to eliminate effects of 60-Hz noise in the laser power), synchronously with the CCD's mechanical shutter opening. Each probe exposure bleached no more than 0.5% of the surface-bound fluorescence per probe frame, as estimated by bleaching surface-bound rhodamine-bovine serum albumin (BSA) under the same conditions. The bleach was accomplished by increasing the illumination duration by a factor of 100–200 for a single flash, without changing the intensity. This protocol allows the use of simple on/off laser shuttering rather than graded analog control of laser intensity and is easier to implement where total laser output power is limited. The average bleach amplitude ranged from 0.5 to 11 counts per pixel in different runs, which gave adequate signal to noise when 5 × 5 pixel groups were fitted. Data were collected at 10 frames/min. The spatially resolved intensities were recorded in a stack of successive CCD image frames.

TIR/FRAP theory

The surface binding/unbinding kinetic equation can be expressed as

$$A + B \underset{k_{off}}{\overset{k_{on}}{\rightleftharpoons}} C \tag{1}$$

where A represents the bulk concentration of free molecules in the cytoplasm, B represents the surface density of free binding sites, and C represents the surface density of surface-bound molecules. Assuming that free actin diffusion is fast compared to its binding/unbinding kinetics (see Appendix A) and that there is only one kinetic process occurring (an oversimplification), then the TIR/FRAP recovery fraction should be 1.0 (i.e., 100% complete), in the shape of a single inverted exponential, where the exponential rate is the off-rate of the surface-bound molecules (Thompson et al., 1981). A recovery fraction of less than 1.0 can be attributed to the presence of a second kinetic process that has a recovery rate slower than the experimental time scale.

Our data fit well to a two-kinetic-rate model: a reversible or "mobile" component with a single inverted exponential, plus an irreversible or "immobile" component with an essentially zero kinetic rate, as shown in Eq. 2:

$$f(t \geq 0) = f_\infty - ae^{-kt} \tag{2}$$

Fig. 4 shows the whole-cell average fluorescence followed frame by frame for a typical TIR/FRAP experiment, with a fit to Eq. 2. A multiple exponential could have been used as a fitting function, but this would introduce degrees of freedom unnecessary to fit our data.

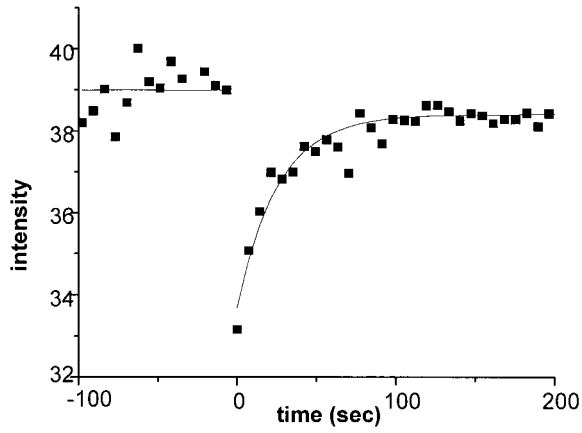

FIGURE 4 Typical TIR/FRAP data with exponential fit (*line*) for a nondisrupted R-actin-labeled control cell. For this particular cell (shown in Fig. 5 *a*), the bleach fraction is 15%, the off-rate k_{off} is 0.040 ± 0.006 s^{-1}, and the mobile fraction α is 0.9.

The cell's fluorescence $f(x, y, t)$ is calculated for each pixel (or binned group of pixels) as a function of time from

$$f(x, y, t) = counts(x, y, t) - dark(x, y) - off\_cell, \quad (3)$$

where the variable $counts(x, y, t)$ is the integral number of counts the CCD camera reports at a particular pixel at a particular time; $dark(x, y)$ is a spatially variable image composed of the average of 30 frames taken in a dark room and representing the readout bias of the CCD camera, which varies with x and y; and *off_cell* is the average fluorescence due to intrinsic glass luminescence and to fluorescent molecules adsorbed to the glass and is determined from a rectangular region in the illuminated area (containing N pixels) that does not contain fluorescence from the cell:

$$off\_cell = (1/N) \cdot \sum_{\substack{\text{in beam} \\ \text{outside of cell}}} [counts(x, y) - dark(x, y)] \quad (4)$$

The intensity represented by *off_cell* does not result from scattering of the evanescent field, inasmuch as it is not altered in the "downstream" direction from possible scattering centers. The variable $f(x, y, t)$ is stored as a real (noninteger) number.

Parameter definitions

The "prebleach intensity," $f(-)$, is the average of ~10 prebleach frames at each pixel location or binned group. The bleach occurs at $t = 0$, the intensity just after the bleach is $f(0_+)$, and the observed postbleach fluorescence for $t > 0$ is $f(t)$. The fit parameters are defined as follows.

The "bleach amplitude" L is defined to be the amount of fluorescence lost as a result of the bleach pulse:

$$L = f(-) - f(0_+) \quad (5)$$

The "mobile fraction" α is the fraction of the bleach amplitude that recovers:

$$\alpha = a/L = [f_\infty - f(0_+)]/L \quad (6)$$

We calculated the mobile fraction from the right-side expression, without reference to fit parameter a, by estimating f_∞ as the average of f in the five last (i.e., largest t) frames to occur.

The "off-rate," k_{off}, is the exponential recovery rate, k, of the fit (Eq. 2). This identification of k as k_{off} depends on the process being in the "reaction limit" rather than the "diffusion limit" (see Appendix A) (Thompson et al., 1981).

The "average off-rate," $\langle k_{off} \rangle$, is the product of the off-rate and the mobile fraction:

$$\langle k_{off} \rangle = \alpha k_{off} \quad (7)$$

The parameters that are of most interest here are α, k_{off}, $\langle k_{off} \rangle$, and $f(-)$. The first three are "kinetic parameters" and should be independent of the illumination intensity, bleach intensity, bound fluorophore distance from the coverslip, or any other nonkinetic variable. One nonkinetic variable, the "bleach fraction" (defined as the normalized bleach amplitude $L/f(-)$) displays an interesting behavior in our data but is more difficult to interpret (see Appendix B).

Analysis methods

The spatially resolved kinetic data were analyzed in several different formats to emphasize particular features. All fitting, analysis, and display software was custom-written in Fortran.

Kinetic parameter spatial maps

Data were binned into nonoverlapping 5×5 pixel groups, equivalent to 1.25 μm on a side, to increase signal to noise. Then the fluorescence average in each pixel group is fit by Eq. 2. This results in hundreds to thousands of fits per cell. Each kinetic parameter resulting from fits of data from individual pixel groups (i.e., α, k_{off}, and $\langle k_{off} \rangle$) can be displayed as a pseudocolor or grayscale spatial map.

Spatial autocorrelations

The spatial autocorrelation function G for a "generic" parameter A was calculated (Wang and Axelrod, 1994) according to

$$G_A(r) = \left[\sum (A(x, y) - \langle A \rangle) \cdot (A(x', y') - \langle A \rangle) \, H(r_1 - r) H(-r_1 + r + 1) \right] \div \left[G_A(0) \sum H(r_1 - r) H(-r_1 + r + 1) \right] \quad (8)$$

where $r_1 = \sqrt{(x - x')^2 + (y - y')^2}$, $\langle A \rangle$ is the average of A over the cell, and $H(s) = 1$ if $s \geq 0$, and $H(s) = 0$ if $s < 0$. The product of the mathematical step functions H ensures that the summation includes only terms representing radial positions in the range $(r, r + 1)$ around any position r'. The spatial autocorrelation function for each parameter characterizes the spatial persistence of deviations from the parameter's average value.

An exponential fit to the spatial autocorrelation function quantitatively reports a characteristic persistence distance d_{corr} (the "correlation distance"), where a nonzero correlation distance indicates that neighboring locations tend to behave similarly. In many cases here, the spatial autocorrelation function did not appear to be exponential, but dipped below zero before returning to or above zero. Nonetheless, all theoretical fits of G to a simple exponential were assumed to decay to zero, with all data values far beyond the zero intercept distance excluded from the fitting procedure. $G(0)$ (which contains a large "shot noise" spike) was also excluded. An approximate "zero intercept distance" d_{zero} was calculated by fitting the points in the spatial autocorrelation function around the first negative point with a linear function. As a control, parameter values were randomly exchanged ("scrambled") among existing locations and then autocorrelated. This control procedure should obliterate the true systematic "signal" while preserving a measure of the expected noise in the autocorrelation function.

Gradient of kinetic parameters

Each spatially resolved parameter α, k_{off}, $\langle k_{off} \rangle$, or $f(-)$ (here again denoted as generic parameter A) was fit to a hypothetical flat plane:

$$A = c + x(m \cos \theta) + y(m \sin \theta) \quad (9)$$

where the "height" of the plane is the parameter value at location (x,y). The maximum slope m of the plane (if significantly nonzero) and its orientation θ reveal the absence or presence of cell-wide trends, e.g., a tendency of one end of the cell to exhibit faster off-rates, for example, than the opposite end. As a control, parameter values were scrambled among existing locations and then fit with a hypothetical flat plane as a measure of expected noise in slope m.

Dependence of kinetic parameters on local brightness

Spatial variations in prebleach fluorescence intensity $f(-)$ could be due to variations in the concentration of surface binding sites, the equilibrium constants of binding at the surface, or the distance from the cytoskeletal protein to the glass. To reveal the presence or absence of correlations between the prebleach intensity and various kinetic parameters, pixels in a TIR/FRAP time sequence image stack were grouped ("binned") according to the average prebleach intensity $f(-)$ of each pixel. The total fluorescence in each such group of pixels was then followed through the TIR/FRAP time sequence and fit according to Eq. 2. The various kinetic parameters were compared for different $f(-)$ bins, and the dependence of the various kinetic parameters upon $f(-)$ was graphed.

Cross-correlations

Cross-correlations can be calculated quantitatively between either 1) two different types of parameters after the same bleaching event (e.g., to determine if brighter locations tend to be less mobile); or 2) parameters of the same type after two different bleaching events (e.g., to determine if the results are repeatable). In general, the cross-correlation $\xi(A,B)$ between the parameters A and B can be calculated by the following equation:

$$\xi(A, B) = \frac{\sum_i (A_i - \langle A\rangle) \cdot (B_i - \langle B\rangle)}{\sqrt{\sum_i (A_i - \langle A\rangle)^2 \cdot \sum_j (B_j - \langle B\rangle)^2}} \qquad (10)$$

where the exact meaning of the summation over i and the averaging denoted by $\langle\ \rangle$ brackets depends on the application. Note that $\xi(A, B)$ is 0 if A and B are uncorrelated, 1 if they are perfectly correlated, and -1 if they are perfectly anticorrelated.

Kinetics averaged over the whole cell

To calculate kinetic rates averaged over each entire cell, the fluorescence signal $f(x, y, t)$ (from Eq. 3) was summed over all x and y and fit by Eq. 2, using the Levenberg-Marquardt algorithm (Press et al., 1994).

Estimated concentration of labeled protein in microinjected cells

For rhodamine-dextran-injected cells, the ratio of the TIR fluorescence intensity from the injected cell (at the brightest locations) versus the same rhodamine-dextran solution deposited straight onto the coverslip was ~0.10, meaning that the cytoplasmic volume was ~10 times the microinjected solution volume. Therefore, because the concentration of injected rhodamine-actin was ~25 μM, the concentration of rhodamine-actin in injected cells is estimated to be on the order of 2 μM. Because the concentration of injected rhodamine-phalloidin was 6–12 μM, its final concentration in rhodamine-phalloidin-injected cells is estimated to be on the order of 1 μM.

RESULTS

Spatially resolved kinetics

Spatial maps

For the seven rhodamine-actin-injected nondisrupted "control" cells, Fig. 5 shows computer-constructed spatial maps of $\langle k_{off}\rangle$ alongside the corresponding TIRF intensity images. The kinetic parameter $\langle k_{off}\rangle$ clearly shows a nonrandom trend in most cells, with one end of the cell typically showing faster average actin kinetics than the other. Typically, the spatial variations in $\langle k_{off}\rangle$ throughout the cell range over an order of magnitude, from ~0.01 to 0.1 s^{-1}. Fig. 6 shows spatial maps of the related kinetic parameters (k_{off} and the mobile fraction α) for one of these cells (cell A). Although trends from one side of the cell to the other are evident, these trends do not obviously correspond with the filamentous structures seen in the TIRF intensity images.

Fig. 7 displays actual TIR/FRAP recoveries from the "fast" and "slow" ends of a rhodamine-actin-injected control cell that exhibits a large gradient in k_{off}; the curves are clearly very different. The particular pixels from the fast and slow regions used for Fig. 7 were selected based on their similar prebleach intensities, so that visual comparisons could be made independently of initial intensity.

To quantitatively characterize the patterns seen in Figs. 4 and 5 and to judge their statistical significance, we performed spatial autocorrelations, cross-correlations, and analysis of cell-wide kinetic gradients as discussed in Materials and Methods.

Autocorrelations

A spatial autocorrelation function of a particular parameter displays the spatial persistence of deviations from the average. Fig. 8 shows the spatial autocorrelation functions for $\langle k_{off}\rangle$ for the seven rhodamine-actin-injected, nondisrupted cells. The correlation distance d_{corr} of $\langle k_{off}\rangle$ is on the order of 2–5 μm (average 3.5 $\pm$ 0.6 μm (SE)). Moreover, $\langle k_{off}\rangle$ shows not just a positive correlation over short distances, but also a negative correlation over larger distances, crossing to a negative correlation at distances d_{zero} ranging from 7 to 14 μm (average 11 $\pm$ 1 μm (SE)), which is a significant fraction of the cell size.

For each experiment type that displays kinetic recovery, and for each kinetic parameter, Table 1 shows the average correlation distances d_{corr} (resulting from an exponential fit to the spatial autocorrelation functions) and zero-crossing distances d_{zero} (resulting from a linear fit as discussed in Materials and Methods). Fig. 6 depicts the d_{corr} lengths of the k_{off} and α spatial maps for one of the cells.

To check against the possibility that the correlations are a calculational artifact, the same analysis was made of existing data sets where the spatially distributed values were scrambled among existing spatial locations. The resulting autocorrelation function fit to a characteristic distance of less than 0.5 μm, with a zero intercept distance of less than 1 μm. Furthermore, the same analysis was done on the point spread function of our optical/CCD setup, which is a Lorentzian of width 1.3 μm. The characteristic distance for the point spread function was 0.6 $\pm$ .04 μm, and the zero intercept distance less than 2 μm. Given the small distances for these control calculations relative to the experimental values, the values in Table 1 do not appear to be artifacts.

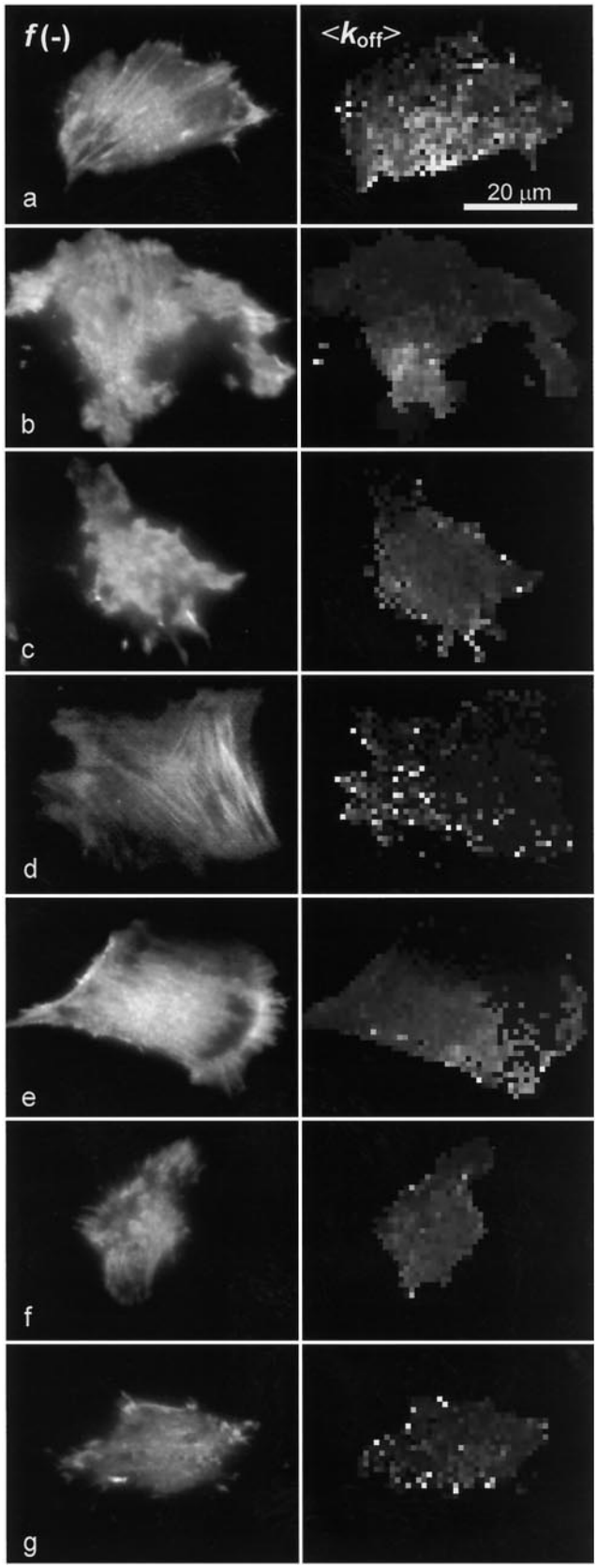

FIGURE 5 TIR prebleach intensity images of the seven R-actin-labeled cells used in nondisrupted control experiments (*left*) and the corresponding spatially resolved maps of $\langle k_{off} \rangle$ (*right*), where each fit region is 4 × 4 pixels (1 μm × 1 μm). Filamentous structures are clearly seen in the TIRF images of cells *a*, *d*, and *e*. The bar represents 20 μm for all panels. The contrast scale for $\langle k_{off} \rangle$ is dark gray = 0, white = 0.1 s^{-1}.

Gradients of kinetic parameters

Spatially dependent data for each particular parameter was fit to the hypothetical plane of Eq. 9. The slope m of the fit plane is the cell-wide gradient of the parameter, i.e., a measure of the polarization of the cell with respect to that parameter. For each of the parameters and for each type of cell treatment that displayed a kinetic recovery, Table 2 summarizes the resulting gradients (both absolute and normalized). Note that the normalized gradient is greater for kinetic parameters than for the prebleach intensity. The orientation angles θ of the gradient axis for the different parameters do not show significant correlation with each other, except for k_{off} and $\langle k_{off} \rangle$, which are generally within 20° of each other. The gradients are statistically significant as judged by two criteria: 1) the fitting errors in the gradients are small compared to the gradient values, and 2) the error bars of the gradient fits to actual kinetic parameter data do not overlap with the error bars of the gradient fits to spatially scrambled data. Fig. 6 shows the direction of the gradient on one particular cell for prebleach intensity, off-rate k_{off}, and mobile fraction α.

Cross-correlations

Significant nonzero cross-correlations occur in rhodamine-actin-labeled cells among pairs of kinetic parameters. Using Eq. 10 with index i referring to 5 × 5 binned spatial locations and $\langle\ \rangle$ referring to a spatial average over the cell, we obtain $\xi = 0.47 \pm 0.18$ for the pair k_{off} and $\langle k_{off} \rangle$, and $\zeta = 0.53 \pm 0.18$ for the pair $\langle k_{off} \rangle$ and α. There is also a slight anticorrelation of $\zeta = -0.16 \pm 0.04$ for the pair k_{off} and α. There is no consistent correlation or anticorrelation between prebleach intensity $f(-)$ and any of the kinetic parameters.

In all of these tests, $n = 7$ and the errors are SE.

In an alternative test of the dependence of kinetic parameters on intensity, data can be grouped by initial intensity; we used five intensity groups for each cell. In each separate group, TIR/FRAP recovery data were averaged and fit. Although some individual cells showed modest but clear trends, there is no consistent sign to the trends for all cells.

Repeatability of spatial patterns

To determine if the spatially resolved variations of kinetic parameters could be measured reproducibly, TIR/FRAP was repeated on the same cell, with the bleaches separated by ~6 min. This was done in four rhodamine-actin-injected

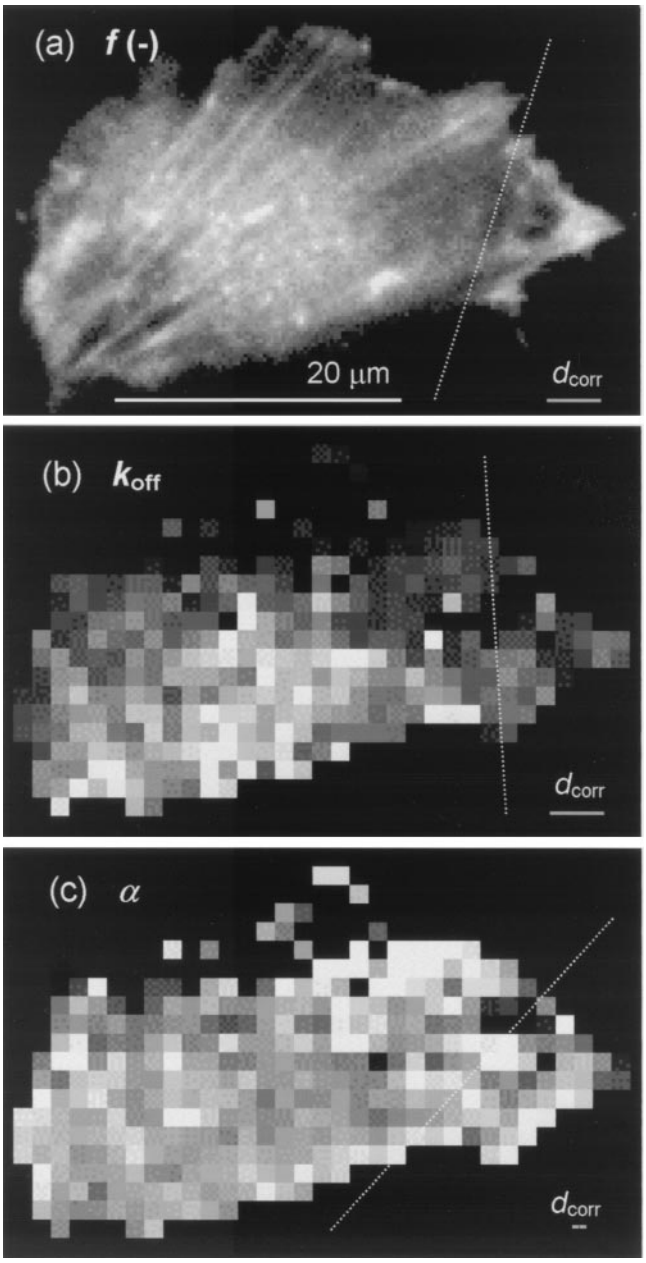

FIGURE 6 Images of the spatially resolved kinetic parameters for a R-actin-labeled cell (cell *a* in Fig. 5). (*a*) Prebleach fluorescence intensity $f(-)$ (no binning). (*b*) Off-rate k_{off} (grayscale range $0-0.1\ s^{-1}$). (*c*) Mobile fraction α (grayscale range 0–1). For the kinetic parameters in *b* and *c*, the pixels are binned 5×5, corresponding to $1.25\ \mu m \times 1.25\ \mu m$ before the data are fit. The long white bar represents 20 μm. The gray bar in the lower right corner of each panel represents the relevant d_{corr} lengths for this cell. The dotted lines in each panel show the orientations of the maximum gradient of a planar fit to the data for $f(-)$, k_{off}, and α, respectively.

control cells. The spatially resolved kinetic parameters were cross-correlated using Eq. 10, where A_i represents a parameter from the first TIR/FRAP experiment at the 5×5 pixel bin centered at (x_i, y_i), and B_i represents the same parameter at the same bin (x_i, y_i) for the second TIR/FRAP experiment

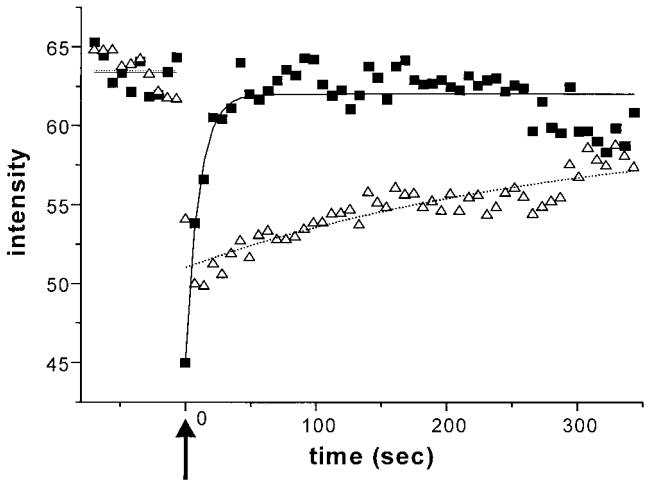

FIGURE 7 TIR/FRAP recoveries from the "fast" (■) and "slow" (△) ends of a particular R-actin-injected cell (cell *a* of Fig. 5), where the "fast" and "slow" ends are identified by a fit to Eq. 9. The bleach time is indicated by an arrow, and the smooth lines represent the computer fits to an inverted exponential. Note that the "slow" end appears to bleach less deeply than the fast end (see Appendix B). The noise in the recovery curves is due to both shot noise (random scatter) and possible small cell motions (infrequent step transitions).

on the same cell, and $\langle\ \rangle$ refers to a spatial average. The resulting cross-correlations ζ ($\pm$ SE) averaged over the four cells are 0.40 ± 0.03, 0.18 ± 0.13, and 0.95 ± 0.05 for k_{off}, α, and $f(-)$, respectively. The agreement in θ (the orientation of the gradient) between the two experiments was high for k_{off}: the average magnitude difference was only $8 \pm 7°$. The average magnitude difference in θ for the α and $f(-)$ were larger ($69 \pm 40°$ and $45 \pm 33°$, respectively) as expected, because the mobile fraction did not exhibit high

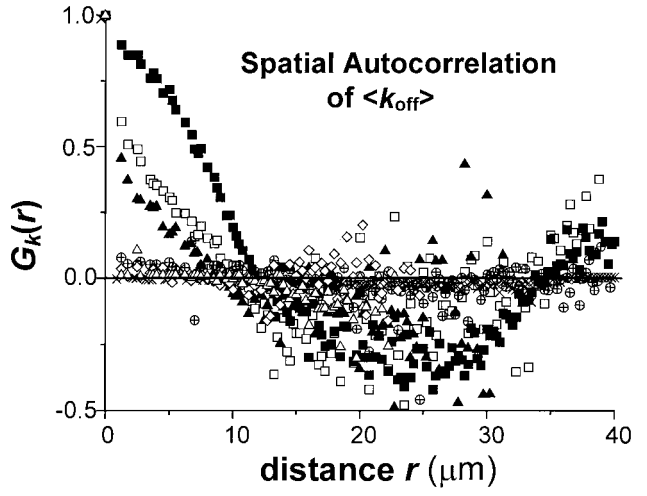

FIGURE 8 Spatial autocorrelation functions $G(r)$ for the average off-rate $\langle k_{off} \rangle$ for the seven R-actin-injected cells depicted in Fig. 5.

TABLE 1 Spatial autocorrelation distances (μm)

Actin marker	$f(-)$		k_{off}		α		$\langle k_{off} \rangle$	
	d_{corr}	d_{zero}	d_{corr}	d_{zero}	d_{corr}	d_{zero}	d_{corr}	d_{zero}
R-actin ($n = 7$)	2.8 ± 0.4	10 ± 1	3.5 ± 0.6	11 ± 1	1.1 ± 0.5	10 ± 1	2.0 ± 0.7	11 ± 1
R-actin + phalloidin ($n = 4$)	3.3 ± 0.3	9 ± 1	1.7 ± 0.4	10 ± 1	1.6 ± 0.3	10 ± 2	1.1 ± 0.4	13 ± 2
R-phalloidin ($n = 4$)	2.4 ± 0.7	8 ± 2	1.8 ± 0.6	7 ± 1	1.5 ± 0.5	7 ± 1	1.9 ± 0.9	7 ± 1

Values listed are spatial autocorrelation distances d_{corr} and d_{zero} for the prebleach intensity and the three kinetic parameters k_{off}, α, and $\langle k_{off} \rangle$.

correlation between bleaches and the intensity did not exhibit a high normalized gradient (see Table 2).

Kinetics averaged over the whole cell

Kinetic rates with and without biochemical disruption

Table 3 shows the mobile fraction α, off-rate k_{off}, and average off-rate $\langle k_{off} \rangle$ for 1) rhodamine-actin-injected cells in the absence and presence of unlabeled phalloidin, cytochalasin B, and sodium azide and 2) rhodamine-phalloidin-injected cells. Rhodamine-actin-injected cells in the absence of further treatment with cytochalasin B or azide generally displayed a significant (one-half to two-thirds) mobile fraction. However, cytochalasin B and sodium azide-treated rhodamine-actin-injected cells displayed a significantly smaller mobile fraction (although with a large cell-to-cell variability in the case of cytochalasin B). Surprisingly, phalloidin had little effect on the fluorescence-marked actin kinetics, regardless of whether labeled or unlabeled phalloidin was used.

There were occasional TIR/FRAP recoveries that were anomalous in one or both of the following ways: the fluorescence at the first point after the bleach was significantly greater than the next two points; and/or the mobile fraction was much greater than 1.0. Both of these characteristics indicate behavior other than equilibrium kinetics. These recovery curves also displayed long recovery time scales, on the order of 200 s or more. The presence of these distinct characteristics made the anomalous recoveries relatively easy to separate out. The fraction of cells displaying anomalous recoveries were: zero of seven for control rhodamine-actin, three of eight for rhodamine-actin with unlabeled phalloidin, and two of seven for rhodamine-phalloidin-labeled cells. This anomalous recovery pattern was also observed in an additional two untreated rhodamine-actin-labeled cells that were operationally identified as "dead" (and not included in the above groups), based on their mottled phase-contrast appearance and spindly semiretracted lamellipodia. Time-lapse phase-contrast movies showed that these two cells were still technically alive. This anomalous (and possibly bleach-induced) phenomenon seems to occur in very stressed cells; however, the mechanisms underlying anomalous recoveries were not investigated further, and the analysis of these curves is not included here.

Calculation of C/A

C/A is the ratio of concentrations of surface bound to free cytoplasmic protein, with units of length. It is essentially the depth in the bulk that contains the same number of labeled molecules as are bound at the surface. *C/A* is a useful quantity because 1) given a characteristic evanescent field depth δ (80 nm in our case), $C/A\delta$ is the fraction of the fluorescence signal that arises from the surface-bound protein; 2) *C/A* can be used to calculate whether the experiment is in the reaction or diffusion limit (Thompson et al., 1981); and 3) *C/A*, together with the measured k_{off}, can be used to calculate the kinetic on-rates. Details of the measurement of *C/A* are given in Appendix A, but the results are presented here. We find that for rhodamine-actin-injected control cells $C/A \geq 30$ nm, and for rhodamine-phalloidin-injected cells $C/A \geq 16$ nm. The lower-bound values are valid under the

TABLE 2 Planar gradients of fits to kinetic parameters

Actin marker	$f(-)$		k_{off}		α		$\langle k_{off} \rangle$	
	m_{abs}	m_{norm}	m_{abs}	m_{norm}	m_{abs}	m_{norm}	m_{abs}	m_{norm}
R-actin ($n = 7$)	0.14 ± 0.03	0.3 ± 0.1	0.0032 ± 0.0004	1.9 ± 0.4	0.019 ± 0.003	0.9 ± 0.1	0.0025 ± 0.0002	2.0 ± 0.3
R-phalloidin ($n = 4$)	0.20 ± .02	0.6 ± 0.3	0.0023 ± 0.0004	1.4 ± 0.3	0.031 ± 0.025	1.4 ± 0.8	0.0068 ± 0.0008	1.3 ± 0.7

Values are planar gradients of fits to the prebleach intensity and the three kinetic parameters, using Eq. 9. The left column for each parameter is the "absolute slope" m_{abs} (s-μm)$^{-1}$, defined as the change of the fit parameter value per micrometer of distance along the steepest gradient. All parameters show statistically significant nonzero m_{abs} values, indicating the presence of a nonzero cell-wide gradient in each parameter. The errors given for m_{abs} are the average of the errors resulting from fits of individual cells and thereby represent the signal-to-noise rather than the cell-to-cell variation for m_{abs}. The right column in each category is a "normalized slope" m_{norm}, defined as the ratio of the highest value of the fit parameter (along the steepest gradient at one end of the cell) minus the lowest value of the fit parameter (at the other end of the cell), all divided by the average value of the kinetic parameter over the whole cell. The normalized slope can be compared between different parameters. The gradient of the initial intensity $f(-)$, for example, is less than one-half the gradient of k_{off}.

TABLE 3 Actin kinetic parameters averaged over the entire cell

Actin marker	Biochemical disruption	k_{off} (±SE) (s^{-1})	α (±SE)
R-phalloidin	—	0.033 ± 0.013 ($n = 5$)	0.66 ± 0.12 ($n = 5$)
R-actin	—	0.032 ± 0.007 ($n = 7$)	0.57 ± 0.08 ($n = 7$)
R-actin	Unlabeled phalloidin	0.016 ± 0.007 ($n = 5$)	0.67 ± 0.15 ($n = 5$)
R-actin	Cytochalasin B	0.20 ± 0.10 ($n = 1$)	−0.15 ± 0.26 ($n = 3$)
R-actin	Azide	0.054 ± 0.01 ($n = 1$)	0.06 ± 0.05 ($n = 3$)

Values are for the two kinetic parameters α and k_{off}, averaged over whole actin-marked cells. Cells treated with cytochalasin B and with azide ceased ruffling and motility motions as judged by time lapse sequences; cells in the other categories retained their motions.

assumptions that the bound protein is at z = 0 and has the same bleachability as rhodamine-bovine serum albumin absorbed to glass in water. At these *C/A* values, exchange of molecules on the surface with those in the bulk would not be limited by bulk diffusion toward the surface in the time ranges of interest here (see Appendix A). Therefore, the TIR/FRAP recoveries observed here are very likely in the "reaction limit," in which the recovery rate is truly a measure of k_{off}. Last, given the measured off-rate k_{off} (see Table 3), the on-rate k_{on}*, defined as $k_{on}B$, is calculated from the quantity $k_{off}C/A$ to be $k_{on}^* \geq 10^{-8}$ cm/s.

Cell-to-cell variations

The error bars of the individual kinetic parameter fits do not overlap for different cells. For example, the average fit error in k_{off} is ±12%, whereas the variations from cell to cell are ± 61% (SD). Each cell generally retained its whole-cell-averaged parameters over two successive TIR/FRAP bleach-recovery cycles. For example, those cells with a generally high k_{off} measured after the first bleach also displayed a relatively high k_{off} measured after the second bleach, where the two bleaches were separated by ~6 min in four control treated rhodamine-actin-injected cells. The cell-averaged kinetic parameters were cross-correlated using Eq. 10, where A_i represents a parameter from the first TIR/FRAP experiment on cell *i* (averaged over the whole cell); B_i represents the same averaged parameter for the second TIR/FRAP experiment on the same cell *i*; and the summation and $\langle\ \rangle$ averages are taken over all of the cells. The cross-correlations are $\zeta = 0.50$ for k_{off} and $\zeta = 0.83$ for α. This implies that at least part of the cell-to-cell variation in the fit parameters reflects some cellular individuality rather than a random instrumental artifact.

Ruling out possible artifacts in the recoveries

Diffusion of fluorophore in the bulk cytosol

The evanescent field, with its 80-nm 1/*e* depth, can excite some cytosolic fluorescence-marked molecules that are near the surface but are not surface bound. These molecules might become bleached during the prolonged bleach illumination pulse, and the fluorescence signal might subsequently recover by diffusion in the bulk. To help rule out the possibility that such a bulk diffusion process contributed to the TIR/FRAP recovery in our experiments, TIR/FRAP was done on cells injected with rhodamine-dextran (MW 70,000) (Molecular Probes), an inert water-soluble polysaccharide larger than an actin monomer. No decrease in fluorescence was observed because of the bleach pulse in rhodamine-dextran-injected cells. This means that the recovery time of the rhodamine-dextran due to diffusion in the cytosol is shorter than our present setup can observe (~1 s), and shorter than the times observed for rhodamine-actin-injected cells. As an additional control intended to show that the bleach pulse was adequate in total energy, bleach of the same intensity was applied to immobile rhodamine-BSA adsorbed irreversibly to a coverslip. A deep bleach was observed, but (as expected) without any recovery.

Reversibility in bleaching or fluorophore attachment

To determine whether our observed fluorescence recoveries might be due to reversible photobleaching or (in the case of rhodamine-phalloidin) reversible attachment of the fluorescent toxin to actin, TIR/FRAP was done on paraformaldehyde-fixed rhodamine-actin- or rhodamine-phalloidin-labeled cells. A significant bleach depth without recovery was observed in both cases. TIR/FRAP was also done on a motionless rhodamine-actin-injected cell (i.e., "dead" as judged by inactivity in time lapse phase contrast). Again, a significant bleach depth without recovery was observed. These results rule out the possibilities that the TIR/FRAP recoveries on unfixed, viable cells are due to reversible photobleaching or reversible attachment of the fluorescent marker.

Faster rates

To rule out the possibility that our setup with its relatively slow CCD camera might obscure a somewhat faster recovery rate, a nonimaging TIR/FRAP setup with a single-channel avalanche photodiode detector (SPCM-100; EG&G Optoelectronics) was utilized at sample bin durations of 40 or 80 ms, a factor of 100 shorter than durations attainable in our CCD-based setup; this setup was able to observe rates

up to $\sim 10\ s^{-1}$. On two different rhodamine-actin-injected cells, the recovery curves fit well to a single exponential with k_{off} of $0.050 \pm 0.008\ s^{-1}$ and $0.023 \pm 0.006\ s^{-1}$; these rates are consistent with the k_{off} rates measured by our CCD setup. Therefore, the actin-marked cells contain no actin kinetic rates up to $\sim 10\ s^{-1}$ that cannot not be recorded in imaging mode by the present CCD camera TIR/FRAP setup.

Photochemical damage

To check for the possibility that light-induced damage might affect the results, a TIR/FRAP experiment was done with one-quarter the usual illumination for both probe and bleach on a rhodamine-actin-injected cell. The measured off-rate of 0.036 ± 0.022 and mobile fraction of 0.7 ± 0.2 agree well with the results obtained with full illumination.

DISCUSSION

Overview

This report describes the first application of TIR/FRAP in imaging mode to living cells, used here to measure actin kinetic unbinding rates ("off-rates") at the submembrane. Regardless of whether the actin in living BC3H1 cells is marked by injected rhodamine-labeled actin monomers or by injected rhodamine-phalloidin, the TIR/FRAP measurements show similar off-rates and fractions of marked actin that are reversibly bound ("mobile fraction"). The kinetic parameters derived from the TIR/FRAP results show considerable variations, both between different cells and spatially within a single cell. However, as could be seen from multiple TIR/FRAP experiments on the same cell, some spatial and cell-to-cell variations are repeatable and consistent features of the cells.

Although different parts of a typical cell show different kinetic rates, the kinetic rates are generally similar over distances on the order of 3 μm. This is quantitatively clear from the spatial autocorrelation functions for initial intensity, mobile fraction, off-rate, and average off-rate, which display a positive correlation over short distances, with a characteristic distance of 1–3 μm, and a negative correlation over larger distances greater than $\sim$7–14 μm. Furthermore, cells exhibited significant cell-wide gradients of kinetic parameter polarity, with an apparent "fast" and "slow" end in the off-rate, mobile fraction, and average off-rate (and also bleach fraction). However, the prebleach fluorescence intensity exhibited somewhat smaller relative cell-wide gradients.

Some cells exhibited a dependence of the off-rate on initial intensity. However, the direction of the dependence was inconsistent from cell to cell. If we simplistically assume that the on-rate and local density of actin-binding sites are spatially invariant, then we might expect that areas with a faster off-rate would coincide with areas of lower prebleach intensity. However, the opposite was true in several cells: brighter locations coincided with faster off-rates. Therefore, the simplistic assumption cannot be true, and therefore the density of actin-binding sites and/or the on-rate must vary spatially in the cell.

In principle, recovery after TIR photobleaching could arise from nonkinetic processes, such as reversible photobleaching, recovery by diffusion, and recovery arising from membrane motion. The first two possibilities were refuted by control experiments. The third appears unlikely because the fluorescence at each pixel after bleach recovery is complete was found to be highly correlated ($\xi = 0.94$) with the prebleach fluorescence at that pixel. If recovery were due to membrane motion, we would expect little correlation between initial and final intensities at particular pixels.

R-Actin kinetics

Theriot and Mitchison (1991, 1992) measured the dissipation times of fluorescence-photoactivated actin from actin filaments in lamellipodia as observed by epiillumination. In two different fibroblast cell lines, actin dissipation times were found to be 55 ± 28 s and 181 ± 99 s. In highly motile goldfish epithelial keratocytes, the actin dissipation time was observed to be 23 s. These dissipation times were reasonably interpreted as the average time in which a marked actin remains incorporated in an actin polymer filament, i.e., the characteristic time for depolymerization. Our TIR/FRAP measurements yielded an average residency time of 31 ± 7 s for actin to remain at or near the cytoplasmic membrane in BC3H1 smooth muscle cells. The characteristic times provided by these two very different techniques might be viewed as "consistent" with each other (although it is surprising that the turnover rates in the keratocytes are not significantly faster than in our less mobile BC3H1 cells). However, the cell types were different (keratocytes, for example, do not have stress fibers), and the optics were different: dissipation of photoactivated fluorescence preferentially probes actin depolymerization in lamellipodia at the cell periphery, whereas TIR/FRAP can probe cell-substrate contact regions underlying even rather thick central parts of a cell.

The time scales of actin kinetics as seen by TIR/FRAP can be compared to time scales of cellular motion. If, for example, actin kinetic time scales are much longer than time scales of cellular motion, then actin binding and unbinding at the cytoplasmic submembrane are probably not involved in cell motility. On the other hand, if the time scales of actin kinetics are short compared to cell motility, then there is ample time for the actin cytoskeleton to reshuffle during the morphological alterations of motility. Of course, the time scale for cellular motion can be a somewhat ambiguous concept because it would depend on an arbitrary assignment of a characteristic distance. We estimated the time scales of

cellular motion by an autocorrelation technique that reports the average time that the local cell boundary remains within ~0.4 μm of its original position, about one pixel here (see Appendix C). Although arbitrary, this characteristic distance is clearly much smaller than any dimension of the cell. In several experiments with four cells, time scales for cell morphological alterations ranged from 50 to 200 s for local motions of <0.4 μm. These time scales are somewhat longer than the actin off-rate, measured as 31 s, thereby allowing for the possibility that the actin cytoskeleton does reorganize with binding/unbinding events during cell motion.

Treatment of rhodamine-actin-injected cells with sodium azide results in a reduction in mobile fraction by a factor of 10. Furthermore, TIR/FRAP on a "dead" cell with no motile activity (shown by a phase-contrast movie) shows zero average kinetic rates. These results confirm that the reversible chemistry of actin at the cell submembrane as detected by TIR/FRAP is an active, energy-dependent process. Patterson and Spudich (1995) have suggested (for a very different cell type, *Dictyostelium*) that azide may disrupt some actin involved in cellular spreading and flattening. In general, stress on the cell (including the response to microinjection itself) may affect the actin network. Treatment with cytochalasin B also results in a 10-fold reduction in the average mobile fraction of injected rhodamine-actin. Cytochalasin B (at much lower concentrations than used here) is known to block polymerization of actin into a filament (at the barbed end) and to decrease interfilament interactions (MacLean-Fletcher and Pollard, 1980). If cytochalasin B decreases the polymerization "on-rate" of monomeric actin onto filaments but the filaments do not change their length by a significant factor (MacLean-Fletcher and Pollard, 1980), then perhaps the off-rate is also reduced. TIR/FRAP directly measures "off-rates"—either marked actin departing from filaments or marked filaments leaving the submembrane under illumination. At our concentrations, it is likely that actin filaments are more extensively disrupted. The cytochalasin B effect seen here may suggest that cytochalasin B at high concentration inhibits the motion of whole filaments.

R-phalloidin kinetics

Phalloidin is a toxin that binds very strongly to polymerized actin, and one might predict that it would inhibit actin binding/unbinding kinetics. According to the results presented here, such is not the case; phalloidin (in either unlabeled or labeled form) does not alter the kinetic off-rate or mobile fraction, relative to rhodamine-actin. Although phalloidin slows locomotion and growth in tissue culture cells in a dose-dependent manner (Wehland et al, 1977; Wehland and Weber, 1981), cells injected with phalloidin still divide and move (Wang, 1987), and phalloidin-labeled f-actin does translocate in a living cell (Wehland et al., 1980). A related actin marker, phallacidin, does not inhibit cytoplasmic streaming in algae (Barak et al., 1980). In our experiments, the injected phalloidin concentration is estimated to be approximately the same as that used by Wang (1987). The similarity of the TIR/FRAP results for fluorescent actin and fluorescent phalloidin suggests that phalloidin can be a good actin marker not just for structure but also for dynamics at the submembrane of living cells.

Such "submembrane dynamics" (as measured by the postbleach fluorescence recovery of R-phalloidin) could arise, in principle, from several phenomena falling into two distinct classes: 1) "actin dynamics" involving either exchange of whole fluorescence-marked actin filaments in the evanescent field or depolymerization of R-phalloidin-bound monomers from actin polymers or 2) "phalloidin dynamics" involving reversible dissociation of R-phalloidin from its actin filament (or other) binding sites. To determine whether our measured results arise from actin dynamics rather than phalloidin dynamics, we can compare our recovery rates to previous measurements of phalloidin association and disassociation rates from filamentous rabbit skeletal muscle actin, reported as 2.9×10^4/M/s and 2.6×10^{-4}/s, respectively (de la Cruz and Pollard, 1996). Based on these figures, phalloidin dynamics would have a characteristic recovery time of ~3000 s, or ~100 times longer than our observed times. We can conclude that phalloidin does not bind to different actin molecules during the course of our experiment, and it is unlikely that the kinetics we observe are phalloidin-actin dissociation dynamics. The kinetic process we observe experimentally with TIR/FRAP on R-phalloidin-injected cells probably results from the motion of entire filaments or protofilaments.

Because phalloidin binds predominately to polymerized actin, the similarity in the time scales of TIR/FRAP results for R-phalloidin and R-actin cells supports this inference that the kinetics (and intensities) provided by the TIR images arise mainly from the motion of entire filaments or protofilaments. This is not to say that monomeric actin does not engage in significant reversible binding activities with nonactin sites at the submembrane, but only that the effects are dominated by polymerized actin, at least in the cells used here.

Using standard spot FRAP on filaments in the cytoplasm of phalloidin-injected Swiss 3T3 cells, Wang (1987) measured the actin recovery time to be 500 $\pm$ 65 s. Based on FRAP diffusion measurements with an epifluorescent focused laser spot, Wang (1987) attributed this process to attachment/detachment of small actin filaments to larger bundles of filamentous actin. Because our measured characteristic time (the reciprocal of the k_{off}) of actin dynamics at or near the cytoplasmic membrane in phalloidin-injected cells was only 30 $\pm$ 12 s, the dynamic rates of phalloidin-labeled actin located deep within the cytosol in Swiss 3T3 cells appear to be an order of magnitude slower than the corresponding rates near the membrane of our BC3H1 cells.

Imaging TIR/FRAP as a technique

In addition to producing spatially resolved data, an imaging mode for TIR/FRAP has several advantages over a nonimaging mode. Imaging mode TIR/FRAP automatically documents the absence of common problems, such as beam drift, focus drift, or changing interference fringes in the illuminating beam, thereby affording higher confidence in the data. The imaging mode also permits both better background subtraction and possible correction of temporal illumination fluctuations by calibration with the background emission intensity in off-cell regions. The imaging mode is also useful for assaying the cellular state during or after experimentation.

There are also some disadvantages to using the imaging mode. The CCD has significant readout noise per pixel for each image, somewhat higher than the noise of a single-channel photodetector (usually a photomultiplier or avalanche photodiode) typically used in nonimaging mode. The second disadvantage of imaging is slower speed; nonimaging mode TIR/FRAP has been used previously at sampling rates as high as 30,000 data bins/s (McKiernan et al., 1997). Both of these problems can be partly ameliorated with newer commercial cooled CCD cameras, which are both quieter and faster than the one used here.

SUMMARY

This paper demonstrates that spatially resolved kinetics can be measured using TIR/FRAP with imaging at the submembrane of living cells. Use of a CCD detector yields orders of magnitude more data than conventional single-channel detectors, from which can be extracted spatial maps and information about cell-wide gradients, dependence of kinetics on initial intensity, and correlations of kinetic parameters with fluorescence structures. This project demonstrates that significant and repeatable variations occur in the kinetic parameters over the surface of the cell and from cell to cell.

Possibile future applications of TIR/FRAP on living cells include the correlation of cell-wide kinetic parameter gradients to external stimulation or cell motion (such as in fast-moving keratocytes); measurements of kinetics of some of the many other submembrane proteins; and comparison of cell-to-cell kinetic variations with the stage of cell division. In particular, TIR/FRAP studies on other proteins crucial to the motile and mechanical properties of the cell surface (such as annexin), but with a less complex (and thereby more interpretable) chemistry or a smaller range of binding sites, appear worthwhile. In addition, the microinjection step may be circumvented in the future by use of cells transfected with genes for specific cytoskeletal protein-green fluorescent protein hybrids.

APPENDIX A: *C/A* RATIO

In the simple $A + B = C$ model of surface binding used here, the surface-proximal C molecules are assumed to be bleachable, and the bulk molecules A are assumed to be effectively unbleachable because of the rapid turnover by diffusion in the bulk. Therefore the observed bleach fraction is affected by *C/A*, the ratio of surface concentration to bulk concentration for fluorescent actin in cells. In principle *C/A* can be calculated by comparing the bleach fraction α in the sample of interest (labeled cells) to the bleach fraction seen for immobile rhodamine-BSA adsorbed to glass at the same bleach intensity and duration, denoted here as α_o (Zimmerman et al., 1990; McKiernan et al., 1997). In general, the observed bleach fraction α will be reduced from α_o by a factor representing the fraction of the fluorescence that is effectively bleachable:

$$\frac{\alpha}{\alpha_o} \leq \frac{F_C}{F_A + F_C} \tag{A1}$$

where F_C represents the fluorescence from C (which is proportional to concentration C), and F_A represents the fluorescence from A (which is proportional to $A \cdot \delta$, where δ is the evanescent field characteristic depth). After substitution of $F_{A,C}$ with their proportional expressions, we can solve for *C/A*:

$$\frac{C}{A} \geq \frac{\delta\alpha}{\alpha_o - \alpha} \tag{A2}$$

The inequalities in Eqs. A1 and A2 arise from the possibly z-dependent distribution of C combined with the exponential dropoff of the evanescent field, which causes fluorophores farther from the surface to bleach less than expected, even if they are immobile. (For example, if the bleach fraction α_o for immobilized rhodamine BSA on glass at $z = 0$ is 0.75, then for rhodamine-BSA distributed evenly and immobilized in the z dimension, the bleach fraction would be only 0.46 for the same bleach duration and intensity.) The equalities in Eqs A1 and A2 hold true only if C is localized entirely at $z = 0$.

In the experimental protocol used here, $\delta = 80$ nm, and the bleach fraction immobilized rhodamine-BSA adsorbed to glass was $\alpha_o = 0.75$. With the same experimental protocol, nondisrupted rhodamine-actin-labeled cells produced an $\alpha = 0.20 \pm 0.02$ ($n = 7$). Substituting these values into Eq. A2 gives $C/A \geq 30$ nm. Similarly, for rhodamine-phalloidin-labeled cells, $\alpha = 0.13 \pm 0.03$ ($n = 5$), giving $C/A \geq 17$ nm.

TIR/FRAP experiments cannot measure kinetic rates faster than "the bulk diffusion limit." The bulk diffusion limit is set by the minimum time required for free unbleached fluorophores to diffuse through the cytosol in sufficient numbers to repopulate the surface. The depth l of cytosol containing the same number of fluorophores as are adsorbed to the surface is $l = C/A$ (as calculated above). The characteristic time t_{diff} for diffusion across this depth is then $l^2/2D$, where D is the diffusion coefficient for free actin monomer in the cytosol (estimated at $\sim 10^{-8}$ cm^2/s). Using $l = 30$ nm (as above), we estimate that $t_{diff} \geq 0.5$ ms, which is a factor of 100,000 shorter than the characteristic time scales observed in actin-labeled cells. Although this result is a lower limit, the magnitude tends to support the view that our experiments are very likely in the reaction limit.

APPENDIX B: BLEACH FRACTION BEHAVIOR

The bleach fraction showed nontrivial spatial patterns and correlations, and the spatially dependent bleach fraction data were analyzed in much the same manner as the off-rate and mobile fraction data. The bleach fraction data are discussed separately here because the results, although statistically significant and interesting, are not unambiguously related to kinetic behavior of the actin at the submembrane. Variations in bleach fraction have previously been observed among different lipid-altered living cells labeled with a plasma membrane dye (Fulbright et al., 1997) and within multinu-

cleated cells labeled with a receptor probe (Axelrod et al., 1976), using spot FRAP.

Spatially dependent bleach fraction variations in rhodamine-actin-injected cells in principle might arise for one or more of the following reasons. 1) Fast moving actin may not reside in the evanescent field for the entire duration of the bleaching pulse; fluorescence at locations with such actin will thereby bleach less than fluorescence at other locations with slower moving actin. However, the actual data do not support this possibility, because the bleach fraction tends to increase with kinetic rate (see below). 2) Locations displaying a higher bleach fraction may represent actin that is closer to the glass substrate, where bleaching rates would be correspondingly greater. The profile of actin concentration versus distance from the substrate will then greatly affect the observed bleachability. 3) Different regions of the cell may have different microenvironments that are associated with different intrinsic bleachabilities. 4) Photochemically induced molecular alterations in the submembrane may affect the apparent bleach fraction if they occur at time scales shorter than the interframe time of our setup. 5) Exchange of bleached fluorophore with unbleached fluorophore (e.g., by free diffusion) on a time scale shorter than the interframe time will decrease the apparent bleach fraction. Further experiments beyond the scope of this study will be needed to distinguish among these possibilities.

The average bleach fractions are similar for rhodamine-actin- and phalloidin-injected cells, and between treated cells and controls. The average bleach fractions in labeled cells are 0.20 ± 0.06 for rhodamine-actin ($n = 7$), 0.13 ± 0.06 for rhodamine-phalloidin ($n = 5$), 0.119 ± 0.004 for rhodamine-actin and phalloidin ($n = 5$), 0.158 ± 0.006 for rhodamine-actin and cytochalasin B ($n = 3$), and 0.161 ± 0.003 for rhodamine-actin and sodium azide ($n = 3$). The bleach fraction agreement between various treatments tends to suggest similarities in bound versus freely diffusing protein ratios and concentration versus z profiles.

The bleach fraction shows a larger variability among different cells rather than within a single cell. For rhodamine-actin, the average intracell standard deviation in the bleach fraction fit was $\pm$ 7%; in contrast, the average intercell standard deviation was $\pm$ 32% from the mean. Cell-to-cell differences in the bleach fraction are repeatable, because multiple bleaches on the same cell show a correlation of 0.62 in the bleach fraction (using Eq. 10, where A_i and B_i are the cell-averaged bleach fractions for the first and second bleaches, respectively, for cell i). Furthermore, the intracell variations are repeatable for multiple bleaches; Eq. 10 yields an average correlation of 0.79 ± 0.13 ($n = 4$) in the bleach fraction (where here A_i and B_i are the bleach fractions at each 5×5 pixel bin i for the first and second bleaches, respectively, in the same cell). These results indicate that both the spatial pattern of the bleach fraction and the cell-to-cell variations in the bleach fraction are repeatable among multiple bleach experiments on the same cell and are not likely to have arisen from noise or experimental error.

The bleach fraction generally displayed distinct spatial patterns. A map representing the spatially resolved bleach fraction for an R-actin-injected cell is shown in Fig. 9. The bleach fraction, like the other parameters, displayed a characteristic correlation distance of ~ 3 μm and anticorrelation greater than ~ 10 μm. In general, the bleach fraction pattern displayed a statistically significant gradient across the cell. By fitting the spatially dependent bleach fraction data to Eq. 9, we could determine if there was agreement in the direction θ of the maximum gradient over successive bleaches on the same cell. The average magnitude difference of θ for the bleach fraction from one bleach to the next was only $4 \pm 3°$.

If the bleach fraction pattern was due simply to the fluorophores' positions in the evanescent field (with more distant fluorophores both dimmer and less bleachable), then we would expect the bleach fraction and the prebleach intensity images to be highly correlated. However, the correlation between mobile fraction and intensity is not consistently significant among all of the cells. However, there is a trend: in locations where the initial intensity is twice as bright (relative to another location), the bleach fraction average increase is a factor of 1.30 ± 0.04 (relative to the other location). This increase is relatively modest, but it is consistent in all of the cells. A positive correlation of bleach fraction with intensity could arise from the position in the evanescent field, but it could also arise from a possible greater bleachability in high local concentrations of fluorophore.

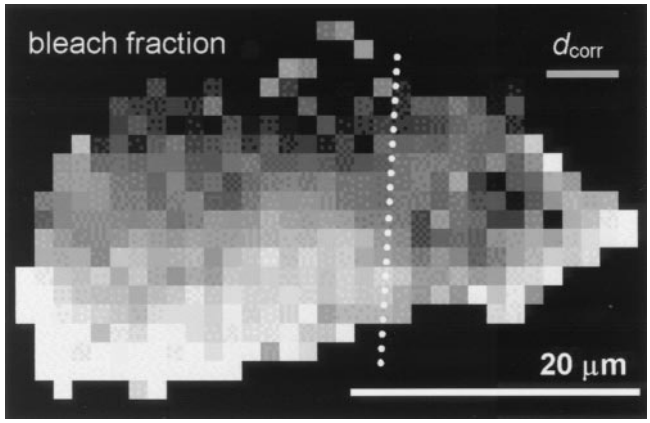

FIGURE 9 Spatial map of the bleach fraction for an R-actin-injected cell (cell *a* of Fig. 5). White represents a bleach fraction of 0.3, and dark gray represents a bleach fraction of 0. The white bar represents 20 μm. The gray bar, showing the calculated spatial autocorrelation distance, represents 3.8 μm. The dotted line indicates the orientation of the maximum gradient of a planar fit (Eq. 9) to the data.

The bleach fraction showed significant correlation with the off-rate and average off-rate. For 5×5 pixel bins, using Eq. 10 with index i referring to 5×5 binned spatial locations and $\langle\ \rangle$ referring to a spatial average over the cell, the cross-correlations were 0.35 ± 0.12 and 0.41 ± 0.04, respectively, for rhodamine-actin-labeled cells ($n = 7$). This signifies that the most bleachable locations tend to recover more rapidly. The bleach fraction did not show consistent, statistically significant correlation with the mobile fraction.

APPENDIX C: RATE OF CELL EDGE MOVEMENT

This appendix describes how time scales of cellular motion are estimated from a time series stack of phase-contrast images. In phase-contrast images, pixels comprising a cell are found to exhibit more intensity variability than pixels comprising the background. A matrix $\mathbf{C}(x,y)$ is meant to reflect the intensity variation between nearby locations; $\mathbf{C}$ is defined to equal the average squared intensity difference between a pixel at (x,y) and all of its nearest neighbors. Because we expect cell locations to exhibit the most intensity variability, "cell locations" are defined to be those for which $\mathbf{C}(x,y) \gg \langle \mathbf{C}_{back} \rangle$, where $\langle \mathbf{C}_{back} \rangle$ is the average of $\mathbf{C}$ in a user-specified background region.

The edge of the cell occurs at cell locations that have two or three, but not one or four, nearest neighbors that are also cell locations. A matrix $\mathbf{E}$ is defined to hold cell edge locations, where $\mathbf{E}(x, y)$ is 1 if this pixel represents a cell edge and is 0 otherwise. (This edge condition is sometimes also true in the interior of the cell; however, these "inside" edge locations were later discarded.).

For a series of N phase-contrast images separated by time τ, the autocorrelation function G calculates the length of time a given edge pixel tends to remain an edge pixel:

$$G(\tau n) = \frac{\sum_{x,y}^{} \sum_{m=1}^{N-n} \mathbf{E}(x, y, m)\mathbf{E}(x, y, m + n)}{\sum_{x,y}^{} \sum_{m=1}^{N-n} \mathbf{E}(x, y, m)^2} \qquad \text{(C1)}$$

For four BC3H1 cells, G was found to exhibit an approximately exponential decay with time scales ranging from 50 to 200 s, meaning that the characteristic time scale of observable motion by the cell edge over a distance corresponding to one pixel is on the order of 50–200 s. Motions larger than one pixel presumably require an even longer time.

We thank Drs. Geneva Omann and James Adams for the gift of fluorescent actin, Dr. Jennifer Linderman for the gift of BC3H1 cells, Dr. Eric Shelden for advice about microinjection, Dr. Richard Hume for advice about microinjection and the use of a micropipette puller, Dr. Pamela Raymond for the use of a micropipette puller, Dr. Fred Lanni for advice about fluorescent actin, Dr. Paul Janmey for information on phalloidin kinetics, Ms. Sharada Kumar for help with cell culturing, and Mr. Keith Shaw and Mr. Alan Kulawik for help with the electronics.

This project was supported by National Science Foundation grant DMB8805292 and National Institutes of Health grant 1R01 NS38129 to DA and a National Institutes of Health/University of Michigan Molecular Biophysics Training grant to SES.

REFERENCES

Axelrod, D. 2000. Total internal fluorescence microscopy. *In* Methods in Cellular Imaging. A. Periasamy, editor. American Physiological Society Book Series, Oxford University Press (in press).

Axelrod, D., E. H. Hellen, and R. M. Fulbright. 1992. Total internal reflection fluorescence. *In* Topics in Fluorescence Spectroscopy, Vol. 3. J. R. Lakowic, editor. Plenum Press, New York. (note that this reference has two misprints: the phase factor of Eq. 7.6 should be $\exp(-i\delta_p)$, and the denominator of Eq. 7.4 should be a square root).

Axelrod, D., P. Ravdin, D. E. Koppel, J. Schlessinger, W. W. Webb, E. L. Elson, and T. R. Podleski. 1976. Lateral motion of fluorescently labeled acetylcholine receptors in membranes of developing muscle fibers. *Proc. Natl. Acad. Sci. USA.* 73:4594–4598.

Barak, L. S., R. R. Yocum, E. A. Nothnagel, and W. W. Webb. 1980. Fluorescence staining of the actin cytoskeleton in living cells with 7-nitrobenzy-2-oxa-1,3-diazole-phallacidin. *Proc. Natl. Acad. Sci. USA.* 77:980–984.

Bloch, R. J., M. Velez, J. G. Krikorian, and D. Axelrod. 1989. Microfilaments and actin-associated proteins at sites of membrane–substrate attachment within acetylcholine receptor clusters. *Exp. Cell Res.* 182: 583–596.

Cooper, J. A. 1987. Effects of cytochalasins and phalloidin on actin. *J. Cell Biol.* 105:1473–1478.

de la Cruz, E. M., and T. D. Pollard. 1996. Kinetics and thermodynamics of phalloidin binding to actin filaments from three divergent species. *Biochemistry.* 35:14054–14061.

Fulbright, R. M., and D. Axelrod. 1993. Dynamics of nonspecific adsorption of insulin to erythrocyte membrane. *J. Fluor.* 3:1–16.

Fulbright, R. M., D. Axelrod, W. R. Dunham, and C. L. Marcelo. 1997. Fatty acid alteration and the lateral diffusion of lipids in the plasma membrane of keratinocytes. *Exp. Cell Res.* 233:128–134.

Gesty-Palmer, D., and N. L. Thompson. 1997. Binding of the soluble, truncated form of an Fc receptor (mouse Fc gamma RII) to membrane-bound IgG as measured by total internal reflection fluorescence microscopy. *J. Mol. Recognit.* 10:63–72.

Gicquaud, C. 1993. Actin conformation is drastically altered by direct interaction with membrane lipids: a differential scanning calorimetry study. *Biochemistry.* 32:11873–11877.

Gicquaud, C. 1995. Does actin bind to membrane lipids under conditions compatible with those existing in vivo? *Biochem. Biophys. Res. Commun.* 208:1154–1158.

Hellen, E., and D. Axelrod. 1991. Kinetics of epidermal growth factor/receptor binding on cells measured by total internal reflection/fluorescence recovery after photobleaching. *J. Fluor.* 1:113–128.

Hsieh, H. V., and N. L. Thompson. 1995. Dissociation kinetics between a mouse Fc receptor (Fc gamma RII) and IgG: measurement by total internal reflection with fluorescence photobleaching recovery. *Biochemistry.* 34:12481–12488.

McKiernan, A. E., R. I. MacDonald, R. C. MacDonald, and D. Axelrod. 1997. Cytoskeletal protein binding kinetics at planar phospholipid membranes. *Biophys. J.* 73:1987–1998.

MacLean-Fletcher, S., and T. D. Pollard. 1980. Mechanism of action of cytochalasin B on actin. *Cell.* 30:329–341.

Pardee, J. D., and J. A. Spudich. 1982. Purification of muscle actin. *Methods Cell Biol.* 24:271–289.

Patterson, B., and J. A. Spudich. 1995. A. novel positive selection for identifying cold-sensitive myosin II mutants in *Dictyostelium. Genetics.* 140:505–515.

Press, W., S. Teukolsky, W. Vetterling, and B. Flannery. 1994. Numerical Recipes in Fortran, 2nd Ed. Cambridge University Press, Cambridge. 678ff.

Sheets, E. D., L. Chen, and N. L. Thompson. 1997. Decreased IgG-Fc gamma RII dissociation kinetics in the presence of a protein antigen. *Mol. Immunol.* 34:519–526.

Simon, J. R., A. Gough, E. Urbanik, F. Wang, F. Lanni, B. R. Ware, and D. L. Taylor. 1988. Analysis of rhodamine and fluorescein-labeled F-actin diffusion in vitro by fluorescence photobleaching recovery. *Biophys. J.* 54:801–815.

Stout, A. L., and D. Axelrod. 1989. Evanescent field excitation of fluorescence by epi-illumination microscopy. *Appl. Opt.* 28:5237–5242.

Tardy, Y., J. L. McGrath, J. H. Hartwig, and C. F. Dewey. 1995. Interpreting photoactivated fluorescence microscopy measurements of steady-state actin dynamics. *Biophys. J.* 69:1674–1682.

Theriot, J. A., and T. J. Mitchison. 1991. Actin microfilament dynamics in locomoting cells. *Nature.* 352:126–131.

Theriot, J. A., and T. J. Mitchison. 1992. Comparison of actin and cell surface dynamics in motile fibroblasts. *J. Cell Biol.* 119:367–377.

Thompson, N. L., T. P. Burghardt, and D. Axelrod. 1981. Measuring surface dynamics of biomolecules by total internal reflection with photobleaching recovery or correlation spectroscopy. *Biophys. J.* 33: 435–454.

Wang, M. D., and D. Axelrod. 1994. Microclustering patterns of acetylcholine receptors on myotubes studied by spatial fluorescence autocorrelation. *Bioimaging.* 2:22–35.

Wang, Y. L. 1987. Mobility of filamentous actin in living cytoplasm. *J. Cell Biol.* 105:2811–2816.

Wehland, J., M. Osborn, and K. Weber. 1977. Phalloidin-induced actin polymerization in the cytoplasm of cultured cells interferes with cell locomotion and growth. *Proc. Natl. Acad. Sci. USA.* 74:5613–5617.

Wehland, J., M. Osborn, and K. Weber. 1980. Phalloidin associates with microfilaments after microinjection into tissue culture cells. *Eur. J. Cell Biol.* 21:188–194.

Wehland, J., and K. Weber. 1981. Actin rearrangement in living cells revealed by microinjection of a fluorescent phalloidin derivative. *Eur. J. Cell Biol.* 24:76–83.

Zimmerman, R. M., C. F. Schmidt, and H. E. Gaub. 1990. Absolute quantities and equilibrium kinetics of macromolecular adsorption measured by fluorescence photobleaching in total internal reflection. *J. Colloid Interface Sci.* 139:268–280.